Chapter 6

Pressure Dependency of the Membrane Structure Parameter and Implications in Pressure Retarded Osmosis (PRO)

Torleif Holt, Edvard Sivertsen, Willy R. Thelin and Geir Brekke

Additional information is available at the end of the chapter

http://dx.doi.org/10.5772/intechopen.72444

Abstract

Pressure retarded osmosis (PRO) can be used to exploit the mixing energy *e.g.* between river water and sea water. A PRO membrane must be highly permeable for water, whereas salt ions should be retained. Furthermore, the structure parameter of the membrane support and backing structure must be low. This paper summarises an assessment of the pressure dependency of the structure parameter for flat sheet membranes, and a transport model for PRO and procedures for determination of the pressure dependency of the structure parameter are presented. The results from laboratory experiments show that that the structure parameter increases significantly with increasing trans-membrane pressure. The increase in the structure parameter was observed to depend on both characteristics of the membrane and the fresh water spacer. Using a finely textured tricot spacer reduced the pressure dependency on the structure parameter, compared to a coarser spacer. Applying a non-woven backing material between the membrane and the fresh water spacer also reduced the impact of pressure. The results show that membranes suitable for river water/sea water PRO must have a sufficiently low structure parameter and additionally resist severe deformation at relevant operating pressures.

Keywords: osmotic power, pressure retarded osmosis, structure parameter, pressure dependence

1. Introduction

Pressure retarded osmosis (PRO) is one feasible technology that can be used to exploit the mixing energy from salt gradients which is commonly referred to as salinity gradient power or

osmotic power [1, 2]. In PRO the transport of water through the membrane is caused by the difference in osmotic pressure across the membrane skin, and the net volume increase on the high saline side due to mass transport against a pressure gradient can be utilised to run a turbine. It should be mentioned that indirect alternatives to exploit the osmotic power, such as osmotic energy recovery in desalination of sea water, have gained increasing attention recently [3–5].

The mass transport of salt and water in PRO can be characterised by three parameters, the water permeability, A, the salt permeability, B, and the structure parameter, S [1, 6]. The parameters must be optimised in order to maximise produced power, implying that the water permeability should be high, and both the salt permeability and the structure parameter should be low. Membrane development has been a prioritised research area for more than a decade, and significant improvements in PRO membrane performance have been achieved over the last years [6–11]. Membrane and element configuration has also been a focus area, and both flat sheet and hollow fibre configurations should be further investigated [12–14].

Resent research has showed that various transport models [14–17] fail to accurately model PRO performance as a function of pressure increase. Kim and Elimelech [18] have related the deviation between observed and modelled performance to adverse effects between the membrane support and the feed channel spacer. Both membrane deformation and obstruction of water permeation were proposed mechanisms to explain the reduced membrane performance at increasing pressures. In case of membrane obstruction, *i.e.* the spacer blocks part of the active membrane area This effect was referred to as the *spacer shadow effect*. Kim and Elimelech showed that the water permeability remained almost independent of the trans-membrane pressure when a diamond shaped feed spacer was applied. On the other hand, the salt permeability increased significantly when the trans-membrane pressure exceeded a certain value (in the range 9–12 bar).

She *et al*. [19] have also studied the impact of spacer characteristics on PRO performance. They showed that mechanical deformation of the PRO membrane did occur during PRO operation. Subsequently, they determined water and salt permeabilities obtained after deformation as a function of trans-membrane pressure in RO experiments, using the same types of feed spacers. Finally, the structure parameter was determined from calculations using the observed water fluxes from the PRO experiments. The variations in the estimated membrane parameters, as well as the mechanical deformation, were found to depend on spacer characteristics.

The interaction between the membrane and the feed spacer is found to reduce the PRO performance of flat sheet membranes. Hollow fibres are self-supporting structures, meaning that the use of spacers is avoided. Any pressure dependency of the PRO performance of hollow fibre membranes must therefore be related to other mechanisms than interactions between membrane and spacer. Chou *et al*. [7] observed a discrepancy between modelled and measured performances for fibres with the skin applied on the bore side. They determined the structure parameter at several pressure steps, and observed that this parameter decreased with increasing pressure. It was suggested that this was due to expansion of the polymer network resulting in reduced tortuosity of the membrane support when the inside of the fibres was pressurised.

The objective of this paper is to present a hypothesis for the interaction between the membrane and spacer which partly builds on the hypothesis of Kim and Elimelech [18]. Based on characterisation experiments we have demonstrated good correlation between measured and modelled membrane performances by applying a pressure dependent structure parameter.

Further, the implications of membrane and spacer interactions in PRO will be discussed and related to the need for optimisation of the characteristic parameters of PRO membranes.

2. Theory

2.1. PRO modelling

A simplified flow diagram indicating main components in a PRO process such as pre-treatment stage, membrane modules, and pressure exchanger, is given in **Figure 1**. In PRO, water will be transported against a pressure gradient due to the difference in osmotic pressure between the draw solution and the feed solution. The net volume increase on the high saline side, which are operated at elevated pressure, can *e.g.* be converted to power in a turbine. The produced power, P, equals the volume flux, J_v, through the membrane, multiplied with the hydraulic pressure difference over the membrane, Δp,

$$P = J_v \Delta p \tag{1}$$

Since the volume of salt transported through the membrane is negligible compared to the volume of water, the volume flux can be replaced by the water flux, J_w.

Different model frameworks describing the transport of salt and water through osmotic membranes have been developed by several authors [15, 20–24]. This paper is based on the stagnant boundary layer model presented by Thorsen and Holt [15], and the basic equations are given below.

Figure 2 shows the cross section of an osmotic membrane in a cross-flow cell, indicating the concentration profile of salt at a given position in the cell, from the fresh water side, through the membrane and to the sea water side.

The transport of water and salt (J_s) through the membrane skin is described by two flux equations, where the positive flux directions are indicated by the arrows in **Figure 2**

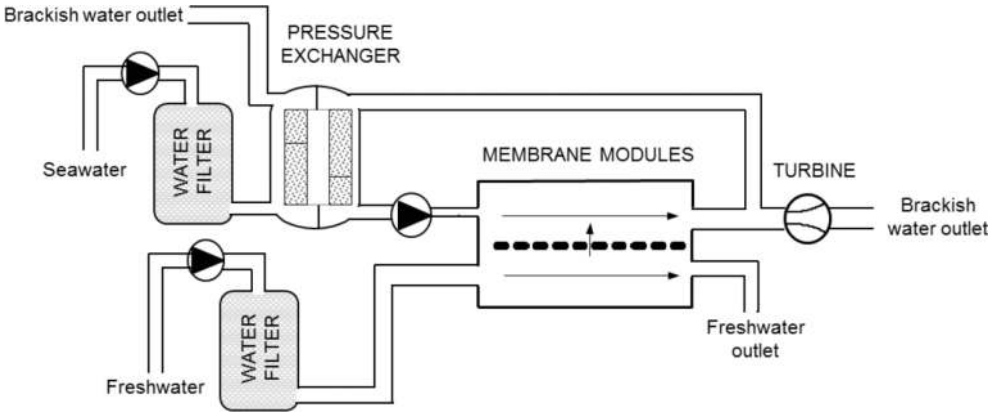

Figure 1. Simplified flow diagram of a PRO power plant.

$$J_w = A(\Delta\pi_{skin} - \Delta p) \tag{2}$$

and

$$J_s = B\Delta s_{skin} = B(c_{sm} - c_p) \tag{3}$$

A and B are the water and salt permeability of the skin, respectively. The osmotic pressure across the skin, $\Delta\pi_{skin}$, is related to the concentration difference $(c_{sm} - c_p)$ of salt over the skin by

$$\Delta\pi_{skin} = iRT(c_{sm} - c_p) = iRT\Delta c_{skin} \tag{4}$$

where i is the van't Hoff coefficient that equals 2.0 for ideal solutions of NaCl. A value of 1.9, which are based on published data for osmotic pressures in NaCl solutions, have been used in the present calculations [25]. R is the universal gas constant and T is the absolute temperature.

The coupled transport of salt in the support membrane and the boundary layers can be expressed by the mass balance

$$-J_s = \frac{\varphi}{\tau} D \frac{dc}{dx} - J_w c \tag{5}$$

where the porosity, φ, and the tortuosity, τ, in the boundary layers on the membrane surfaces equals unity. D is the diffusion coefficient of salt (NaCl). Inserting the water flux in Eq. (2) and the salt flux in Eq. (3) into the mass balance in Eq.(5) and evaluating the transport of water

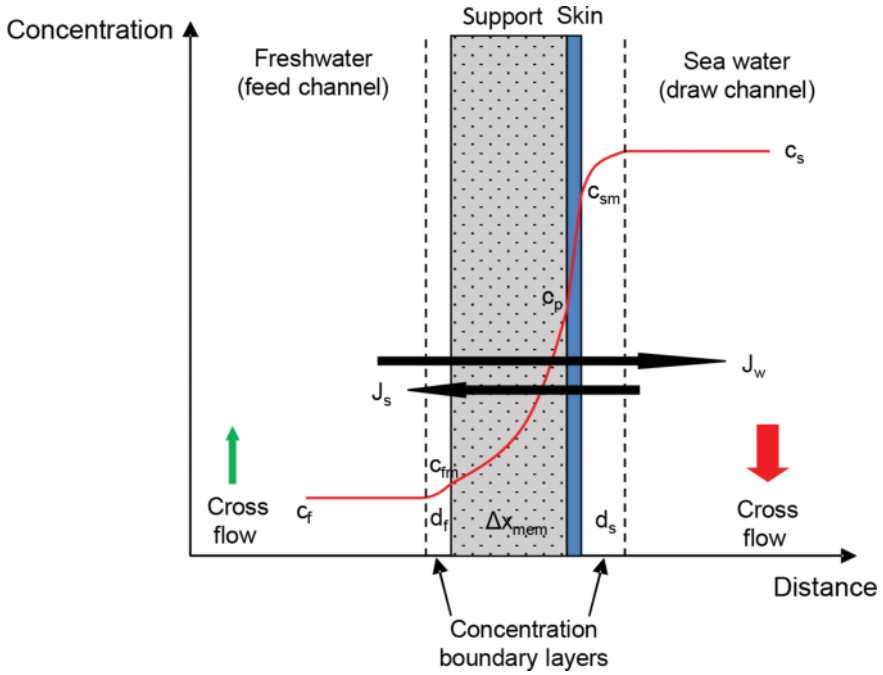

Figure 2. Concentration profile over the membrane and boundary layers.

and salt in the different transport zones results in five equations containing five unknown parameters, J_s, J_w, c_{fm}, c_p and c_{sm}. After some rearrangement, the following expression for the concentration difference across the skin, Δc_s can be found:

$$\Delta c_{skin} = \frac{c_s - c_f e^{\left\{\frac{(S+d_s+d_f)J_w}{D}\right\}}}{e^{\left(\frac{d_s J_w}{D}\right)} + \frac{B}{J_w}\left(e^{\left\{\frac{(S+d_s+d_f)}{D}\right\}} - 1\right)} \tag{6}$$

The equation relates the concentration difference of salt over the membrane skin to the bulk concentrations of salt, and furthermore to the characteristic membrane parameters, as well as the boundary layer thickness on each side, d_s and d_f, respectively. The structure parameter, S, of the membrane support is defined as

$$S = \frac{\tau}{\Phi}\Delta x_{mem} \tag{7}$$

where Δx_{mem} is the thickness of the support membrane that for practical purpose will equal the measured membrane thickness. The salt flux can be found by multiplying Eq. (6) by B.

The water flux can be found by combining Eqs. (2), (4) and (6) giving

$$J_w = A\left(iRT\frac{c_s - c_f e^{\left\{\frac{(S+d_s+d_f)J_w}{D}\right\}}}{e^{\left(\frac{d_s J_w}{D}\right)} + \frac{B}{J_w}\left(e^{\left\{\frac{(S+d_s+d_f)}{D}\right\}} - 1\right)} - \Delta p\right) \tag{8}$$

which is valid when the salt water faces the skin side of the membrane, *i.e.* PRO mode.

2.2. Pressure dependency of the structure parameter

The left sketch in **Figure 3** illustrates the cross section of a PRO membrane at zero trans-membrane pressure. The support membrane rests on the top of the filaments of the feed spacer. The contact area between the membrane and the spacer will in such case be low, and the presence of the spacer material has little or no impact on the mass transfer. An eventual impact will be included in the structure parameter determined by modelling of isobaric experiments.

When pressure is applied on the skin side in a PRO experiment the pressure will exert a force on the membrane, such that feed spacer will be squeezed into the support membrane. This situation is illustrated in **Figure 3** (right sketch). As a result, the membrane may be deformed, and the contact area between the membrane and the feed spacer might increase. Furthermore, the properties of the support structure, such as porosity and interconnections between pores, might be affected. The net effect of these phenomena can be modelled as an increased structure parameter.

A simple equation has been developed in order to illustrate the pressure dependency on the structure parameter and the implicit effect on the water flux:

$$S = S_0\frac{1}{1 - \left(F\Delta p/\Delta p_{ref}\right)} \tag{9}$$

where S_0 is the structure parameter at zero trans-membrane pressure, Δp. Arbitrarily values for the constant F were selected, and constant Δp_{ref} was set to 10.6 bar. As shown in **Figure 4**, the increase in the structure parameter is modest at low trans-membrane pressures, but increases rapidly at higher pressures. The water flux will be reduced when the structure parameter increases. The effect is more pronounced for higher F values.

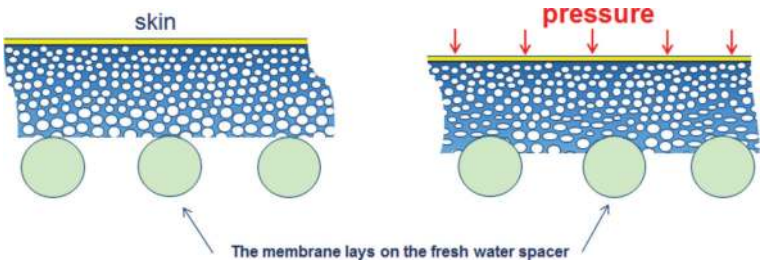

Figure 3. PRO membrane and spacer material at isobaric conditions (left) and pressurised conditions (right). The pores (illustrated by white circles) in the support membrane and possible reinforcement are interconnected giving continuous transport paths.

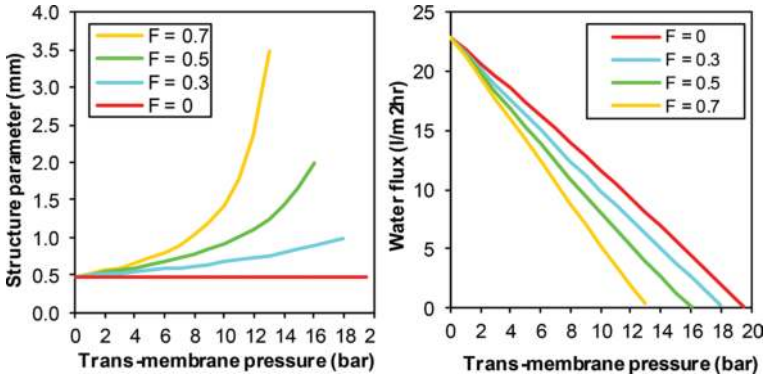

Figure 4. Structure parameters modelled as function of trans membrane pressure according to Eq. (9).

3. Experimental

3.1. Apparatus

All results presented in this work were obtained from measurements performed with two small cross-flow units as illustrated in **Figure 5**. Two membrane cells with different effective membrane area of 6.1 and 9.5 cm^2, respectively, were applied. The channel width was 1.1 cm and the depth of the draw channel was 0.07 cm for both cells. The depths of the feed channels for the two different cells were 0.1 and 0.05 cm, respectively. The draw channels were filled with a 0.07 cm thick diamond spacer, whereas different types of spacers were used in the feed channels.

Both feed and draw solution were pumped through the cross-flow cell using dual-piston pumps with displacement volumes of approximately 10 ml/stroke. The fluids were fed into the pumps from reservoirs placed on balances, and subsequently recycled back to the reservoirs. The cross-flow cells and up-stream tubing were immersed in temperature controlled water baths to maintain the temperature at 20°C during the experiments. The pressures, *p*, the

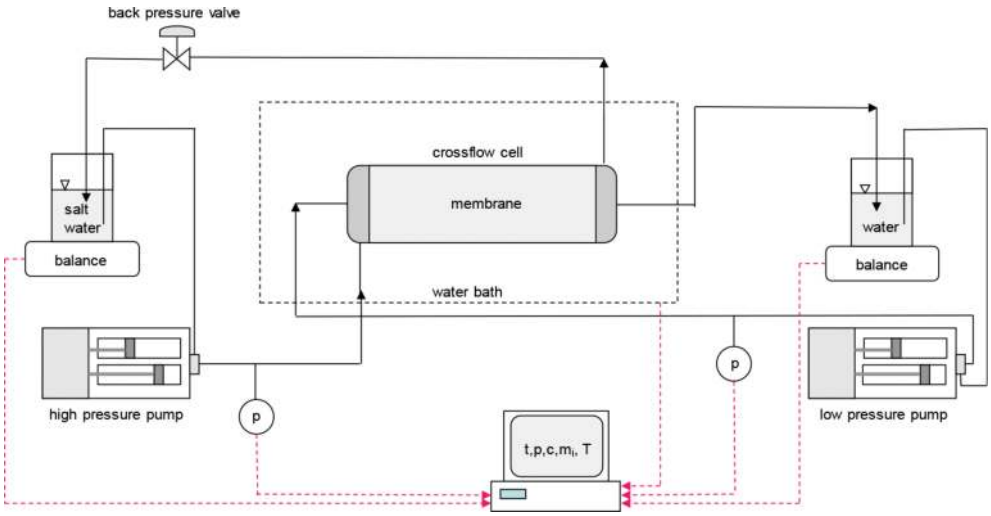

Figure 5. Simplified flow diagram for the two cross flow apparatuses used in the study.

temperature in the water bath, T, and the readings of the balances, m_i, were monitored and logged at regular intervals, t. An inline conductivity cell enabling the determination of the salt concentration in the fresh water, c, was not used in the present experiments.

3.2. Membranes and feed water spacers

The membranes used in this study include one CTA membrane and two TFC membranes (TFC1 and TFC2) from Hydration Technology Inc. and one TFC membrane (TFC3) from Nitto Denko. It should be noted that TFC1 and TFC2 are the first and second generation of the same membrane.

A relatively coarse tricot spacer with 0.5 mm thickness has been used as feed water spacer in our standard test protocols. In addition, some experiments were performed with a finer tricot spacer with 0.25 mm thickness. Photos of both types of spacers are shown in **Figure 4**.

3.3. Test protocol

The salt water solutions were made by dissolving NaCl (p.a.) in degassed (vacuum) and purified water. Degassed and purified water was also used as feed solution in the PRO experiments, and for all pre-treatment and rinsing steps.

If prescribed by the manufacturer, the membranes were pre-treated by immersion in a fluid of composition specified by the membrane manufacturer (often 50 vol. % methanol) for a prescribed time (typically 30 to 300 seconds). Subsequently, the samples were immersed in purified water for minimum 60 minutes prior to assembly in one of the membrane cells. The membranes that were not pre-conditioned were immersed in purified water prior to assembly in one of the membrane cells, in some cases combined with vacuum degassing of the sample.

After assembly, a hydraulic water permeability test was performed. The water flux was measured for minimum four pressure steps, ranging from 1 to 10 bar. Each pressure step lasted for minimum 1 hour. Subsequently, two independent osmotic flow experiments were performed at isobaric conditions. The first experiment was performed in FO mode, *i.e.* draw solution against the membrane support, followed by a second experiment in PRO mode, *i.e.* draw solution against the membrane skin. The cross-flow cell and tubing was flushed with purified water between each experiment.

3.4. Experimental conditions

For the osmotic experiments, the flow velocities (based on open channel) were 1.08 and 0.76 cm/s for the draw channel and the feed channel, respectively, unless stated otherwise. These flow velocities are in the same order as expected flow velocities in a full-scale membrane module for sea water/fresh water PRO. For the hydraulic water permeability experiments, purified water was supplied to both sides of the membrane.

During the osmotic experiments both sides of the membrane were conditioned at ambient pressure by bypassing the back-pressure valve shown in **Figure 5**. During the hydraulic water permeability experiments, and some of the PRO experiments, the back-pressure valve was used to regulate the applied pressure on the draw side. However, most PRO experiments were performed using a closed draw solution loop instead of the back-pressure valve. The closed draw solution loop was continuously pressurised by the volume increase in the draw solution loop.

4. Data analyses and modelling

4.1. Flux and permeability calculations

The water flux was determined based on mass changes in the feed reservoirs. The reported water fluxes were estimated based on the initial phase in each experiment, *i.e.* during the first 1 to 2 hours, before dilution of the draw solution and salt accumulation in the feed solution influenced the mass transport. Hydraulic water permeabilities were calculated from the hydraulic permeability experiments. The salt fluxes were determined by potentiometric analyses of Cl^- ions in a sample collected in the feed reservoir at the end of each experiment. The measured average salt fluxes were corrected to initial conditions using the ratio between initial and average salt concentration differences across the membrane.

4.2. Determination of A, B and S from isobaric osmotic flow experiments

A, *B* and *S* were determined for each membrane by modelling of two isobaric osmotic flow experiments ($\Delta p = 0$). The two experiments, one performed in FO mode and one in PRO mode, produced one water flux and one salt flux each that were used as input to the transport model described in Section 2. Further, *A*, *B* and *S* was determined as the combination of parameters resulting in the minimum sum of squared relative deviations between measured and modelled fluxes. Of the four fluxes that were obtained from the two osmotic flow experiments, three of them are independent, which corresponds to the minimum degrees of freedom required for the parameter estimation. All experiments were modelled by using a boundary layer thickness of 40 μm [26].

4.3. Modelling of PRO experiments

In order to assess the specific power production as function of applied pressure each experiment was divided into pressure steps. The water and salt fluxes, and the salt concentrations on both sides of the membrane, were calculated by mass balances for each pressure step, using the membrane parameters determined for the applied membrane, according to Section 4.2.

4.4. Determination of pressure dependency of the structure parameter

In order to assess the pressure dependency of the structure parameter, S was allowed to increase with pressure. Thus, the modelling procedure described in Section 4.2 was repeated for each pressure step. However, with the distinction that A and B were kept constant and equal to the values determined at isobaric conditions, whereas only the structure parameter was fitted to minimise the sum of squared relative deviations between measured and modelled fluxes.

5. Results and discussion

5.1. Modelling of PRO experiments with constant S

Figure 7 shows the water flux and specific power as function of trans-membrane pressure for two CTA membranes with imbedded reinforcement. The membranes originated from two different production batches. Symbols correspond to experimental data, whereas lines correspond to modelled values which are based on the characteristic membrane parameters determined from the osmotic flow experiments.

It can be observed from **Figure 7** that the measured water fluxes, and thus the specific power, were not very high, which is typical for asymmetric membranes. Furthermore, a significant deviation between measured and modelled performance was observed at increasing trans-membrane pressure.

5.2. Modelling of PRO experiments with pressure dependent S

Figure 8 shows the same experiments as presented in **Figure 7** with the distinction that the modelled values were obtained by using a pressure dependent structure parameter. The pressure dependent structure parameter obtained for the two CTA membranes is plotted as function of trans-membrane pressure in **Figure 9**.

It can be observed that the structure parameter increases significantly with increasing pressure for both membrane samples. Further, the observed variation in the structure parameter with trans-membrane pressure resembles the proposed behaviour given by Eq. (10).

Figure 10 shows the water flux and specific power as function of trans-membrane pressure for two parallel runs with a TFC membrane with imbedded reinforcement, denoted as TFC1. The modelled values were obtained by using a pressure dependent structure parameter. Note that the difference in salt concentration across the membrane skin at maximum specific power was 26.4 and 28.2 g/l for Experiment 1 and Experiment 2, respectively, which explains the observed difference in performance for the two experiments.

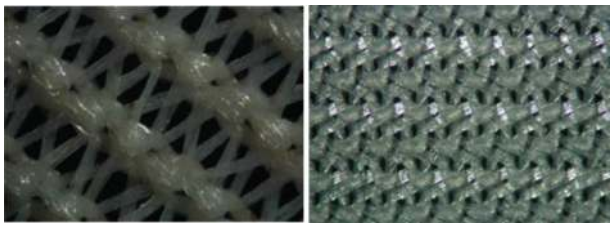

Figure 6. Top view of the tricot spacers used in the feed channel. Left: coarse spacer of 0.5 mm thickness. Right: Fine spacer of 0.25 mm thickness. Photos are shown at the same scale.

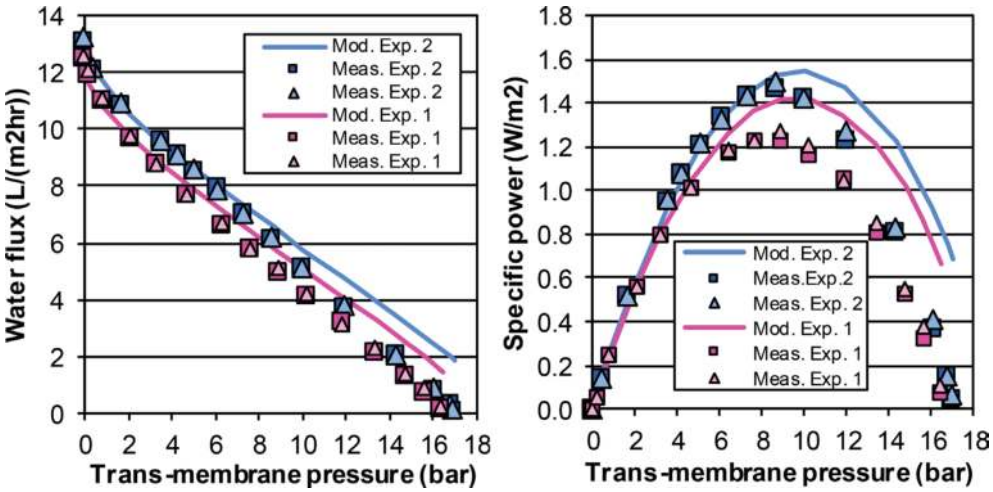

Figure 7. Water flux and specific power as function of trans-membrane pressure for CTA membranes. Modelled values were obtained by applying constant structure parameter determined at isobaric conditions.

Figure 11 shows the pressure dependency of the structure parameter for the two experiments performed with TFC1. Generally, it was observed that the structure parameter of the TFC1 membrane was less affected by pressure than the CTA membrane. *E.g.* at 10 bar the *S* value of the TFC1 membrane was doubled compared to isobaric conditions, whereas the increase in *S* value at 10 bar for the CTA membrane was in the range of 400%.

5.3. Impact of flow velocity on the pressure dependency of S

Table 1 summarises a series of PRO experiments, each performed with different cross-flow velocities and using the membrane denoted TFC2. Experiments 5 and 9 were both performed at standard conditions. The maximum specific power, P_{max}, and the difference in salt concentration across the membrane at maximum specific power, Δc at $P_{max,}$ are given in the table, as well as the pressure found by extrapolation of the water flux vs. the trans-membrane pressure curve to zero water flux, p_{osm}. The latter is commonly referred to as the practical osmotic pressure.

http://dx.doi.org/10.5772/intechopen.72444

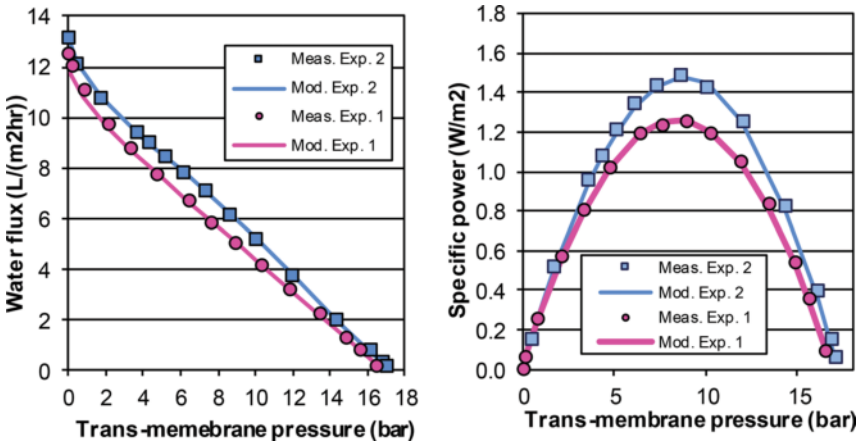

Figure 8. Water flux and specific power as functions of trans-membrane pressure for CTA membranes. Modelled values were obtained by applying a pressure dependent structure parameter.

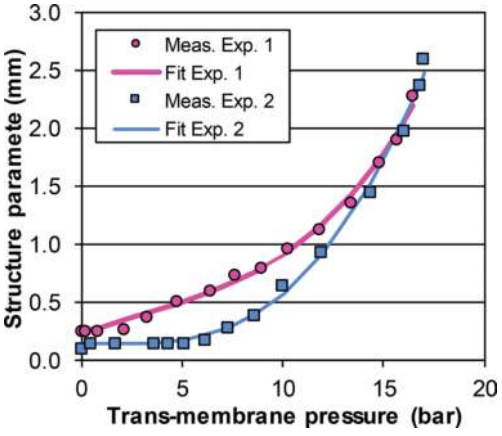

Figure 9. Modelled structure parameter as function of trans-membrane pressure for CTA membranes.

All experiments were modelled according to the procedure described in Section 4.4, and the respective pressure dependent structure parameters are shown in **Figure 12**.

From the reported specific power data in **Table 1** it was observed that the TFC2 membrane (second generation) performed significantly better than the TFC1 membrane (first generation). Further, the results from Experiment 5 and Experiment 9 performed at identical conditions are very similar and indicate good reproducibility.

Comparing the pressure dependency of the structure parameter for the two different TFC membranes in **Figure 12** and **Figure 11**, it was observed that the structure parameter of the TFC2 membrane was less influenced by increasing trans-membrane pressure. Further, the

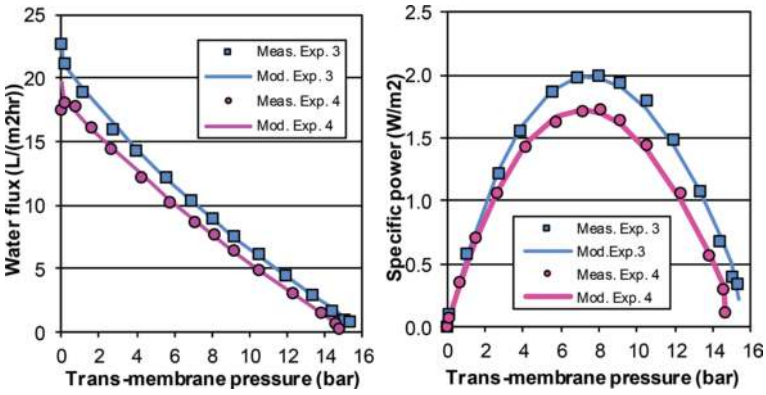

Figure 10. Water flux and specific power as functions of trans-membrane pressure for the TFC1 membrane. Modelled values were obtained by applying a pressure dependent structure parameter.

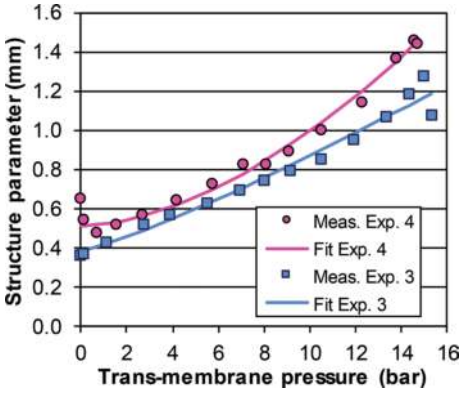

Figure 11. Structure parameters as functions of trans-membrane pressure for the TFC1 membrane.

Exp.	u_{draw} (cm/s)	u_{feed} (cm/s)	P_{max} (W/m²)	Δc at P_{max} (g/L)	p_{osm} (bar)
5	1.08	0.76	3.4	27.2	18.5
6	1.62	1.14	3.8	27.4	18.8
7	2.16	1.52	4.0	27.2	19.5
8	3.25	2.27	4.2	27.4	19.5
9	1.08	0.76	3.4	27.4	18.5

Table 1. Summary of PRO experiments performed with the TFC2 membrane and variable cross-flow velocities.

increase in structure parameter with increasing trans-membrane pressure was observed to have relatively identical slopes for all experiments performed with the TFC2 membrane. Additionally, the structure parameter was observed to decrease at increasing flow velocities.

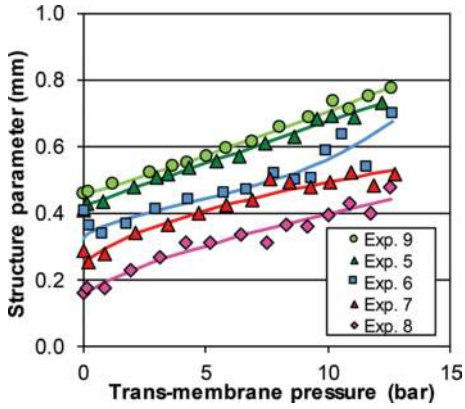

Figure 12. Pressure dependent structure parameters as functions of trans-membrane pressure for the TFC2 membrane.

Figure 13 illustrates the membrane and the feed channel in a cross-flow cell. Since the support membrane is a porous structure some water might be anticipated to flow in the longitudinal direction inside the support membrane as illustrated by the red arrows. The flow velocity inside the support membrane and the penetration depth for the longitudinal flow inside the support will depend on the cross-flow rate, as well as both the flow resistance in the spacer material and in the support membrane, respectively.

For low cross-flow rates and for feed spacers with low pressure drop, the pressure gradient in the feed channel will be small, and little or no water will flow in the longitudinal direction inside the support membrane. At higher cross-flow rates, the pressure gradient in the membrane support will increase, and a significant flow of water inside the support membrane may occur. This will reduce the magnitude of the structure parameter since the effective diffusion length will be reduced when the support structure become more saturated.

Even if high cross-flow velocities may improve mass transfer through the membrane by the effects discussed above, such measure will require increased pumping energy and additionally result in lower utilisation of the feed solution. It should be noted that large pressure losses are unacceptable in sea water/fresh water PRO, and sufficiently low pressure losses are important factors to be considered during development and design of membrane modules for application in PRO plants.

5.4. Impact of spacer selection on the pressure dependency of S

Table 2 summarises results from PRO experiments performed with the TFC3 membrane that was produced without fabric reinforcement.

Two different feed spacers having different thickness and structure were tested. Both spacers were of the tricot type. The feed spacer of 0.25 mm thickness had a much finer structure with smaller distance between the filaments (*cf.* **Figure 6**). Note that experiments 12–15 were performed with the same membrane sample, and between each experiment the membrane cell was opened in order to enable replacement of the feed spacer. Further, a Hirose Histar 15-TH48 (HH 15-TH48) non-woven fabric was placed between the membrane and the feed spacer in

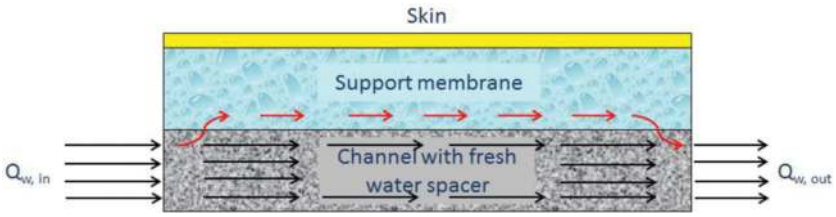

Figure 13. Flow conditions in the fresh water channel and support membrane.

Exp.	P_{max} (W/m^2)	Δc at P_{max} (g/L)	p_{osm} (bar)	Feed water spacer	Extra fabric	Comment
10	3.5	28.1	14.7	0.50 mm	None	
11	4.5	27.4	18.0	2·0.25 mm	None	
12	4.6	27.1	19.0	2·0.25 mm	HH 15-TH48	
13	4.9	28.1	21.5	2·0.25 mm	HH 15-TH48	
14	4.3	28.3	20.0	0.50 mm	HH 15-TH48	
15	4.6	28.1	21.7	2·0.25 mm	HH 15-TH48	Spacer inv.

Table 2. Summary of PRO experiments with the TFC3 membrane.

order to assess if improved support to the membrane did influence membrane compaction, and the resulting increase in the structure parameter. Experiments 10 and 11 were performed with different membrane samples. The pressure dependent structure parameter was calculated for each experiment according to the procedure described in Section 4.4 and is shown in **Figure 14**.

The modelled structure parameter in the experiments performed with the 0.5 mm thick spacer was observed to increase more rapidly with increasing pressure compared to the experiments performed with the less coarse spacer of 0.25 mm thickness. Comparing the two experiments performed with the 0.5 mm spacer it was observed that the introduction of the extra non-woven fabric reduced the observed pressure dependency of the structure parameter. This indicates that improving the support for the membrane does influence the compaction of the membrane structure and the resulting increase in the structure parameter at elevated pressures.

The positive impact on the pressure dependency of the structure parameter by including the extra non-woven fabric was also observed for the experiments performed with the 0.25 mm feed spacer. The structure parameter of the fabric was estimated to 0.13 mm by performing independent salt diffusion experiments. The additional transport resistance exerted by the non-woven fabric can be recognised in the modelled structure parameter as the reinforcement layer ideally should add 0.13 mm to the isobaric structure parameter. This increment was not observed in Experiment 12; however, the deviation is within the expected uncertainty found in the pressure dependent structure parameters.

In Experiment 15, the feed spacer was inverted such that the "flat" side was facing the membrane, resulting in a slightly higher structure parameter compared to the experiments performed with normal orientation of the spacer.

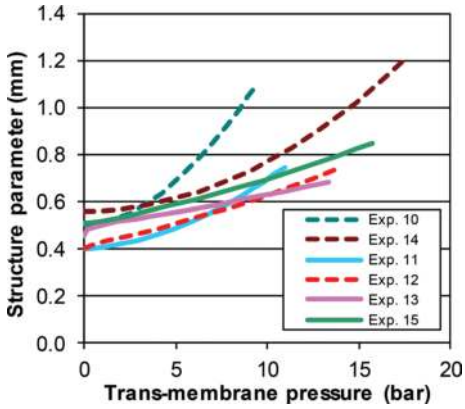

Figure 14. Structure parameter as function of trans-membrane pressure for the TFC3 membrane.

These results show that the extent of support for the membrane is crucial for the PRO performance. It was observed that the coarser spacer resulted in both a faster and a larger increase in the structure parameter at increasing pressure, compared to the more fine-structured spacer providing more support to the membrane. Similar behaviour has been observed in multiple experiments performed with different types of PRO membranes, and agrees well with recent literature [27]. The effect of introducing the extra reinforcement was observed to be larger for the coarser spacer.

5.5. Proposed measures to improve PRO performance at elevated pressures

In order to promote a high specific power in sea water/fresh water PRO, the structure parameter must be low, preferably less than 0.5 mm. The isobaric structure parameters measured for many existing membranes are well below this value. However, when pressurised, an excessive increase in the structure parameter have been observed for many potentially good PRO membranes. An improved strength of the support membrane which is more resistant to compression will therefore be required.

The results in **Figure 14** suggest that one approach to reduce the pressure dependency of the structure parameter might be to apply fine textured feed spacers. However, this will result in increased pressure drop in the feed channel, which might drastically reduce the net produced power in a PRO plant. Even the relatively coarse 0.5 mm feed spacer used in the present work will result in an unacceptable pressure loss. Thus, it should be investigated if it is possible to cast the support membrane directly on a feed spacer, possibly a fine textured tricot type. Supposing that this is viable, two membrane sheets may be separated by *e.g.* a simple diamond type spacer ensuring reasonable low frictional losses.

5.6. Uncertainty in experiments and modelling

The calculation of pressure dependent structure parameters in this paper were based on the assumption that the water and salt permeability were independent of the applied pressure, which may appear to be somewhat contradictory to part of the literature [18, 19]. Nevertheless, our assumption is based on several arguments. (1) In the presented work, the

Exp.	A_{leak}/A (%)	Exp.	A_{leak}/A (%)	Exp.	A_{leak}/A (%)
1	4.9	6	0.1	11	−3.1
2	4.2	7	−0.5	12	0.1
3	5.7	8	−0.6	13	−0.3
4	2.8	9	−1.0	14	0.1
5	0.2	10	−2.5	15	−0.1

Table 3. Hydraulic leakage relative to water permeability.

PRO experiments were performed with a tricot type feed spacer that has been found to result in the lowest variation in the modelled membrane parameters due to variations in trans-membrane pressures [19], and (2) initial water permeability tests using pressures up to 10 bar were performed prior to all PRO experiments. Thus, any membrane deformation that could be expected to influence the skin properties of the membrane as a result of pressurisation should have occurred during the water permeability tests. And (3) the obtained water permeability that were calculated at several pressure steps for each membrane were found to be independent of trans-membrane pressure.

At the end of each PRO experiment the amount of salt on the feed side was determined and compared with the amount of salt calculated by using the transport model. If an excess of salt was determined this was attributed to a hydraulic leakage, and subsequently a leakage volume was calculated by assuming zero salt rejection for the leakage. A leakage permeability, A_{leak}, was calculated based on the leakage volume, duration of the experiment, and average pressure during the experiment. The leakage permeabilities determined for the various experiments are given in **Table 3**. The total leakage volume was distributed for each pressure step based on the duration and average pressure of the step. The salt concentrations on each side of the membrane were subsequently recalculated resulting in new water and salt fluxes, and finally an updated value of excess salt was determined. The calculations converged quickly, and the excess salt was normally low, indicating no (negative leakage volume and thus negative ratio) or only minor leakages.

6. Conclusions

The pressure dependency of the structure parameter in PRO has been investigated for flat sheet membranes, and a transport model including procedures for determination of the pressure dependency of the structure parameter have been presented.

The results from laboratory experiments show that the structure parameter increases significantly with increasing trans-membrane pressure. This was the case both for the CTA membrane and the three TFC membranes that were tested, however, the impact of pressure on the structure parameter was found to be larger for the CTA membrane. Furthermore,

the increase in the structure parameter was observed to depend on the type of feed spacer. Using a finely textured spacer of the tricot type reduced the impact of pressure on the structure parameter in comparison to a coarser spacer material. Applying a non-woven backing material between the membrane and the fresh water spacer was also observed to reduce the impact of pressure on the structure parameter. These results show that developing membranes with sufficiently low structure parameter for pressures relevant for PRO will rely on the membrane's ability to resist deformation during compression. The type of feed spacer is another factor which is crucial to avoid deformation and the resulting increase in the structure parameter at elevated pressures.

The results also showed that increased flow velocities in the feed channel and the draw channel, respectively, will improve the mass transfer of water through the membrane. This might be partly ascribed to reduced concentration polarisation on the membrane surfaces. It is also suggested that high pressure gradients in the feed channel may result in convective flow in parts of the support membrane, improving the mass transfer conditions further. However, large frictional losses in the flow channels, will drastically reduce the net produced power in a sea water/fresh water PRO plant, and must be avoided. This will limit the choice of feed spacers that can be used for PRO.

Nomenclatures

A	water permeability (m/s/Pa)
A_{leak}	hydraulic leakage permeability (m/s/Pa)
B	salt permeability (m/s)
c_f	bulk concentration at the fresh water side (g/l)
c_{fm}	surface concentration at the fresh water side (g/l)
c_p	concentration at the interface between the skin and the porous support (g/l)
c_s	bulk concentration at the salt water side (g/l)
c_{sm}	surface concentration at the salt water side (g/l)
Δc_{skin}	concentration difference across the membrane skin (= $c_{sm} - c_p$) (g/l)
D	diffusion coefficient (m^2/s)
d_s	salt water film thickness (m)
d_f	freshwater film thickness (m)
F	constant in Eq. (10)
i	corrected van't Hoff coefficient (−)

J_V	volume flux (m/s)
J_w	water flux (m/s)
J_s	salt flux (mol/m^2/s)
P	specific power (W/m^2)
P_{max}	maximum specific power (W/m^2)
p_{osm}	practical osmotic pressure (bar)
Δp	trans-membrane pressure (bar)
Δp_{max}	maximum trans-membrane pressure (bar)
Δp_{ref}	reference pressure in Eq. (10) (bar)
$Q_{water,in}$	volumetric flow of water entering a module (−)
$Q_{water,out}$	volumetric flow of water exiting a module (−)
R	universal gas constant (J/K/mol)
S	structure parameter (m)
S_0	isobaric structure parameter (m)
T	absolute temperature (K)
u_{draw}	empty channel velocity at draw side (cm/s)
u_{feed}	empty channel velocity at feed side (cm/s)
x	direction perpendicular to the membrane surface (m)
Δx_{mem}	membrane thickness (m)

Greek letters

τ	tortuosity (−)
φ	porosity (−)
$\Delta\pi_{skin}$	osmotic pressure difference across the membrane skin (bar)

Author details

Torleif Holt[1]*, Edvard Sivertsen[2], Willy R. Thelin[2] and Geir Brekke[3]

*Address all correspondence to: Torleif.Holt@sintef.no

1 SINTEF Petroleum, Trondheim, Norway

2 SINTEF Building and Infrastructure, Trondheim, Norway

3 Statkraft AS, Oslo, Norway

References

[1] Skilhagen SE, Dugstad JE, Aaberg RJ. Osmotic power—Power production based on the osmotic pressure difference between waters with varying salt gradients. Desalination. 2008;**220**:476-482. DOI: 10.1016/j.desal.2007.02.045

[2] Logan BE, Elimelech M. Membrane-based processes for sustainable power generation using water. Nature. 2012;**488**:313-319. DOI: 10.1038/nature11477

[3] Touati K, Tadeo F, Elfil H. Osmotic energy recovery from reverse osmosis using two-stage pressure retarded osmosis. Energy. 2017;**132**:213-224. DOI: 10.1016/j.energy.2017.05.050

[4] Bajraktari N, Helix-Nielsen C, Madsen HT. Pressure retarded osmosis from hypersaline sources—A review. Desalination. 2017;**413**:65-85. DOI: 10.1016/j.desal.2017.02.017

[5] Attarde D, Jain M, Singh PK, Gupta SK. Energy-efficient seawater desalination and wastewater treatment using osmotically driven membrane processes. Desalination. 2017; **413**:86-100. DOI: 10.1016/j.desal.2017.03.010

[6] Sivertsen E, Holt T, Thelin WR, Brekke GM. Iso-watt diagrams for evaluation of membrane performance in pressure retarded osmosis. Journal of Membrane Science. 2015;**489**:299-307. DOI: 10.1016/j.memsci.2015.04.042

[7] Chou S, Wang R, Fane AG. Robust and high performance hollow fiber membranes for energy harvesting from salinity gradients by pressure retarded osmosis. Journal of Membrane Science. 2013;**448**:44-54. DOI: 10.1016/j.memsci.2013.07.063

[8] Yip YN, Tiraferri A, Phillip WA, Schiffman JD, Hoover LA, Kim YC, Elimelech M. Thin-film composite pressure retarded osmosis membranes for sustainable power generation from salinity gradients. Environmental Science & Technology. 2011;**45**:4360-4369. DOI: 10.1021/es104325z

[9] Han G, Zhang S, Li X, Chung TS. High performance thin film composite pressure retarded osmosis (PRO) membranes for renewable salinity-gradient energy generation. Journal of Membrane Science. 2013;**440**:108-121. DOI: 10.1016/j.memsci.2013.04.001

[10] Han G, Wang P, Chung TS. Highly robust thin-film composite pressure retarded osmosis (PRO) hollow fiber membranes with high power densities for renewable salinity-gradient energy generation. Environmental Science and Technology. 2013;**47**:8070-8077. DOI: 10.1021/es4013917

[11] Zhang S, Sukitopaneenit P, Chung TS. Design of robust hollow fibre membranes with high power density for osmotic energy production. Chemical Engineering Journal. 2014; **241**:457-465. DOI: 10.1016/j.cej.2013.10.063

[12] Kim YC, Elimelech M. Potential of osmotic power generation by pressure retarded osmosis using seawater as feed solution. Analysis and experiments. Journal of Membrane Science. 2013;**429**:330-337. DOI: 10.1016/j.memsci.2012.11.039

[13] Sivertsen E, Holt T, Thelin WR, Brekke GM. Pressure retarded osmosis efficiency for different hollow fibre membrane module flow configurations. Desalination. 2013;**312**:107-123. DOI: 10.1016/j.desal.2012.11.019

[14] She QH, Jin X, Tang CY. Osmotic power production from salinity gradient resource by pressure retarded osmosis: Effects of operating conditions and reverse solute diffusion. Journal of Membrane Science. 2012;**401**:262-273. DOI: 10.1016/j.memsci.2012.02.014

[15] Thorsen T, Holt T. The potential for power production from salinity gradients by pressure retarded osmosis. Journal of Membrane Science. 2009;**335**:103-110. DOI: 10.1016/j.memsci.2009.03.003

[16] Yip NY, Elimelech M. Thermodynamic and energy efficiency analysis of power generation from natural salinity gradients by pressure retarded osmosis. Environmental Science & Technology. 2012;**46**:5230-5239. DOI: 10.1021/es300060m

[17] Tiraferri A, Yip NY, Phillip WA, Schiffman JD, Elimelech M. Relating performance of thin-film composite forward osmosis membranes to support layer formation and structure. Journal of Membrane Science. 2011;**367**:340-352. DOI: 10.1016/j.memsci.2010.11.014

[18] Kim YC, Elimelech M. Adverse impact of Feed Channel spacers on the performance of pressure retarded osmosis. Environmental Science & Technology. 2012;**46**:4673-4681. DOI: 10.1021/es3002597

[19] She Q, Hou D, Liu J, Tan KH, Tang CY. Effect of feed spacer induced membrane deformation on the performance of pressure retarded osmosis (PRO): Implications for PRO process operation. Journal of Membrane Science. 2013;**445**:170-182. DOI: 10.1016/j.memsci.2013.05.061

[20] McCutcheon JR, Elimelech M. Modeling water flux in forward osmosis: Implications for improved membrane design. AICHE Journal. 2007;**53**:1736-1744. DOI: 10.1002/aic.11197

[21] McCutcheon JR, Elimelech M. Influence of concentrative and dilutive internal concentration polarization on flux behavior in forward osmosis. Journal of Membrane Science. 2006;**284**:237-247. DOI: 10.1016/j.memsci.2006.07.049

[22] McCutcheon JR, Elimelech M. Forward (direct) osmosis desalination using polymeric membranes. Abstracts of Papers of the American Chemical Society. 2004;**228**:261

[23] Tang CY, She QH, Lay WCL, Wang R, Fane AG. Coupled effects of internal concentration polarization and fouling on flux behavior of forward osmosis membranes during humic acid filtration. Journal of Membrane Science. 2010;**354**:123-133. DOI: 10.1016/j.memsci.2010.02.059

[24] Tang WL, Ng HY. Concentration of brine by forward osmosis: Performance and influence of membrane structure. Desalination. 2008;**224**:143-153. DOI: 10.1016/j.desal.2007.04.085

[25] Dytnerskij JI. Membranprozesse—Theorie und Berechnung. Moskau: Verlag Chimija; 1986. p. 254

[26] Sivertsen E, Holt T, Thelin WR, Brekke GM. Modelling mass transport in hollow fibre membranes used for pressure retarded osmosis. Journal of Membrane Science. 2012;**417-418**: 69-79. DOI: 10.1016/j.memsci.2012.06.014

[27] Sim J, Koo J, Nam S, Kim E, Hwang TM. Effect of combined positions of feed spacer-type tricot on the performance in pressure retarded osmosis (PRO). Desalination and Water Treatment. 2017;**77**:63-68. DOI: 10.5004/dwt.2017.20667